Laser and Particle Beams (2007), *25*, 371–377. Printed in the USA.

DOI: 10.1017/S0263034607000249

Collimated attosecond GeV electron bunches from ionization of high-Z material by radially polarized ultra-relativistic laser pulses

A. KARMAKAR AND A. PUKHOV
Institut für Theoretische Physik I, Heinrich-Heine-Universität-Düsseldorf, Düsseldorf, Germany
(RECEIVED 26 February 2007; ACCEPTED 20 April 2007)

Abstract

Three dimensional Particle-in-Cell (3D-PIC) simulations of electron acceleration in vacuum with radially polarized ultra-intense laser beams have been performed. It is shown that single-cycle laser pulses efficiently accelerate a single attosecond electron bunch to GeV energies. When multi-cycle laser pulses are used, one has to employ ionization of high-Z materials to inject electrons in the accelerating phase at the laser pulse maximum. In this case, a train of highly collimated attosecond electron bunches with a quasi-monoenergetic spectra is produced. A comparison with electron acceleration by Gaussian laser pulses has been done. It is shown that the radially polarized laser pulses are superior both in the maximum energy gain and in the quality of the produced electron beams.

Keywords: Electron acceleration; Ionization; Laser plasma; Three-dimensional particle-in-cell simulation

1. INTRODUCTION

Since the invention of the chirped pulse amplification (Strickland & Mourou, 1985), the laser technology was continuously developing and has lead to focused pulse intensities of 10^{22} W/cm^2 recently (Bahk *et al.*, 2005). Moreover, there are projects to develop lasers producing a few cycle pulses at petawatt (10^{15} W) (Fuerbach *et al.*, 2005), and even exawatt (10^{18} W) power level (ELI Project). One of the most important applications for such short ultra-intense laser pulses (Strickland & Mourou, 1985; Bahk *et al.*, 2005) is the acceleration of charged particles (Pukhov, 2003), both electrons and ions (Yin *et al.*, 2006).

Presently, electron energies from 100 MeV (Mangles *et al.*, 2004; Gedder *et al.*, 2004; Faure *et al.*, 2004) up to GeV (Leemans *et al.*, 2006; Glinec *et al.*, 2005; Koyama, 2006; Lifshitz *et al.*, 2006) have been achieved in the bubble regime of particle acceleration in plasmas (Pukhov & Meyer-ter-Vehn, 2002). When the laser pulse propagates in plasmas, its transverse electric field is converted into the longitudinal field of the plasma wave, which accelerates the particles. However, the next generation of the short pulse lasers is designed to achieve focal intensities of 10^{24} W/cm^2, or even higher. The natural question is arising if these laser fields can accelerate particles to high energies directly, without any conversion to plasma fields.

In this paper, we perform three-dimensional particle-in-cell (3D-PIC) simulations of electron acceleration in a vacuum with radially polarized ultra-intense laser beams. It is shown that single-cycle laser pulses efficiently accelerate a single attosecond electron bunch to multi-GeV energies. When the laser pulse is longer and consists of several cycles, one has to use ionization of high-Z materials to inject electrons in the accelerating phase at the laser pulse maximum. In this case, a train of highly collimated attosecond electron bunches with quasi-monoenergetic spectra are produced. The radially polarized laser pulse is compared with the usual Gaussian pulse. It is shown that the radially polarized laser pulses are superior both in the maximum energy gain and in the quality of the produced electron beams. The reason is the unique field structure of the radially polarized beams that confines the accelerated electrons and keeps them tightly focused near the optical axis over the full acceleration stage.

Although some semi-analytical studies of electron acceleration with radially polarized electron beams have been published in the last few years (Varin & Piche, 2002; Salamin, 2007; Kawata *et al.*, 2005), here we present the first full electromagnetic 3D PIC simulations. The 3D PIC

Address correspondence and reprint requests to: Alexander Pukhov, Institut für Theoretische Physik I, Heinrich-Heine-Universität-Düsseldorf, 40225 Düsseldorf, Germany. E-mail: pukhov@tp1.uni-duesseldorf.de

code Virtual Laser Plasma Lab (VLPL) (Pukhov, 1999) solves the full set of Maxwell equations. In addition, we have incorporated the Monte-Carlo ionization module that allows us to simulate tunnel ionization of deep electron levels of various high-Z materials.

The most important result of this paper is that one needs electron injection via tunneling ionization into the high-intensity center of the multi-cycle laser pulse to achieve high energy gains. When low-Z materials are used, the target is completely ionized by the very foot of the laser pulse. The electrons are trapped by the low intensity part of the laser pulse and never experience the high-field middle of the pulse. As a consequence, electron energy gains are low. The situation changes when high-Z materials are used. If some deep electron shells of the high-Z material survive the laser field, electrons are injected at the laser pulse maximum and experience high energy gains. We show that the electron energy spectra contain quasi-monoenergetic features corresponding to ionization of different electronic shells of the high-Z material.

The paper is organized as follows. The first section describes the implementation of the tunnel ionization module in the code VLPL. The second section presents 3D PIC simulation results and the third section gives discussion and outlook.

2. IMPLEMENTATION OF TUNNELING IONIZATION IN VLPL

VLPL is a relativistic fully electromagnetic PIC code, written using strongly object oriented programming and parallelized using message passing interface (MPI) (Pukhov, 1999). Up to 10^9 particles and 10^8 mesh cells can be used with the single processor performance 0.5 μs/particle, linearly scalable up to several hundreds nodes. VLPL solves the full sets of Maxwells equation of motion of particles. The object oriented configuration allows easy and effective modifications of algorithms.

In VLPL ionization module, both barrier suppression (BSI) and tunneling ionization have been taken into account depending on the laser pulse intensity. The key dimensionless parameter that distinguishes between multi-photon and optical field ionization (OFI) is the Keldysh parameter $\Gamma = \sqrt{I_p/\varepsilon_{os}}$ (Keldysh, 1965). Here I_p is the ionization potential and $\varepsilon_{os} = e^2E^2\ (1+\alpha^2)/4m\omega^2$ is the quiver energy of an electron, α is the polarization parameter, and ω is the laser frequency (Pukhov, 2003). In our paper, we consider laser intensities well above $\sim 10^{16}$ W/cm^2, leading to $\Gamma \ll 1$. Thus, we work in the OFI regime, i.e., tunneling and BSI.

The tunneling regime corresponds to low frequency laser fields, $\hbar\omega \ll I_p$, where I_p is the ionization potential. The field must be smaller than the atomic field $E \ll E_a$, where E_a is the atomic field at the corresponding electron orbit. We calculate the ionization probability in the tunneling regime according to the Ammosov-Delone-Krainov (ADK) (Ammosov *et al.*, 1986) model.

$$W[s^{-1}] = \omega_A C_{n*l} f(l,m) I_p \left(\frac{3E}{\pi(2I_p)^{3/2}}\right)^{1/2} \times \left[\frac{2}{E}(2I_p)^{3/2}\right]^{2n^*-|m|-1} \exp\left(-\frac{2}{3E}(2I_p)^{3/2}\right), \quad (1)$$

where $\omega_A = 4.134 \times 10^{16}\ \mathrm{s}^{-1}$ is the atomic unit of frequency, E is the laser field in atomic units. The factors f and C are given by

$$f(l,m) = \frac{(2l+1)(l+|m|)!}{2^{|m|}(|m|)!(l-|m|)!},$$

and

$$C_{n*l} = \left(\frac{2e}{n^*}\right)^{n^*} \frac{1}{(2\pi n^*)^{1/2}}.$$

Here n^* is the effective principal quantum number, l and m are magnetic and orbital quantum numbers, and e is the Euler number.

The validity of the ADK theory improves as n^* increases (Augst *et al.*, 1991). This occurs for atoms with high atomic numbers and higher charge states, and in our work, we focus exactly at these atoms. Further, we introduce the critical electric field $E_{crit} = I_p^2/4Z$ (Augst *et al.*, 1991), where I_p is the ionization potential, and Z is the atomic number corresponding to the threshold laser intensity

$$I_{th}(\mathrm{W/cm^2}) = 4 \times 10^9 \frac{I_p^4(\mathrm{eV})}{Z^2}.$$

This critical field distinguishes between the tunneling ionization and BSI. For multiple-electron atoms, we implement the sequential ionization only. This means that at every time step, only the bound electron with the lowest ionization potential can be released. For high-Z materials, we use the calculated ionization potentials from the atomic data table (Carlson *et al.*, 1970).

3. SIMULATIONS OF ELECTRON ACCELERATION

To simulate the laser acceleration of electrons in a vacuum we use the 3D PIC code VLPL with the ionization module as explained in the previous section. The simulation box is $X \times Y \times Z = (10 \times 30 \times 30)\lambda^3$, where $\lambda = 0.82$ μm is the assumed laser wavelength. The simulation domain is sampled with the grid of $200 \times 150 \times 150$ cells.

The laser pulse is either linearly polarized Gaussian, or is radially polarized. It propagates in the x-direction. The target is located short in front of the laser focal plane (see Fig. 1). It is a tiny spherical droplet of radius 200 nm and atomic density $n = n_c$, where $n_c = mc\omega^2/4\pi e$ is the critical

https://doi.org/10.1017/S0263034607000249 Published online by Cambridge University Press

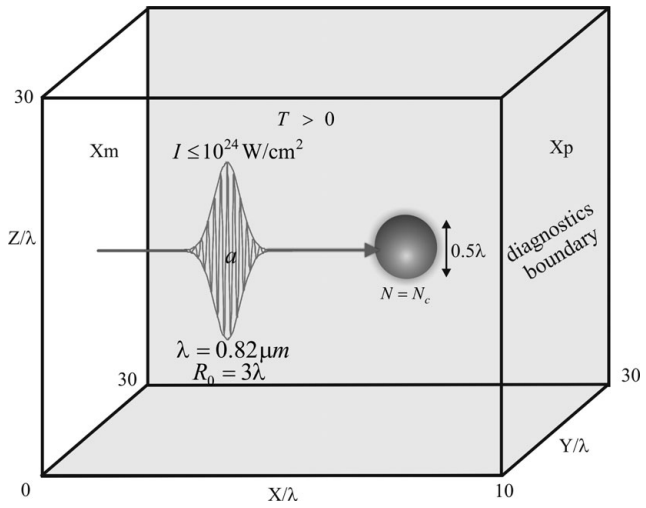

Fig. 1. Geometrical perspective of the 3D PIC simulation.

density. As the laser pulse reaches the droplet, electrons are trapped, and accelerated forward. At this time, the moving window technique is applied and the simulation box follows the relativistic electron bunches. In the simulation, we use 28 atoms or ions per cell. Each atom with Z bound electrons can emit all these during the tunneling or barrier suppression ionization. A single run took around 2 h on 32 Intel-Xeon processors.

We were looking for materials with large enough ionization potentials to survive laser fields as high as $10^{24}\,\mathrm{W/cm^2}$ (ELI Project). Our choices were Xe and Cu, because the I_p for Xe^{52+} is 39.25 KeV and for Cu^{28+} 11.17 KeV (Carlson *et al.*, 1970). We compare these two materials with hydrogen, where $I_p = 13.6$ eV. Hydrogen is, of course, ionized completely by the very foot of the laser pulse. Earlier, electron injection into high-intensity Gaussian laser pulses via ionization has been discussed elsewhere (Hu & Starace, 2002, 2006). Here, we show the difference between the simple Gaussian laser pulses and the radially polarized pulses.

3.1. Radially polarized laser pulse

Here we present simulation results of a radially polarized laser pulse. At the focal plane, the transverse (radial) component of the laser pulse is

$$E_r = E_0 \frac{r}{\sigma_0} \exp(-r^2/\sigma_0^2) \exp(-t^2/T^2) \cos(\omega t), \qquad (2)$$

where σ_0 is the focal spot waist, and T is the pulse duration. The corresponding longitudinal *X*-component of the laser field at the focal plane is

$$E_x \approx E_0 \frac{1}{k\sigma_0} \left(1 - \frac{r^2}{\sigma_0^2}\right) \exp(-r^2/\sigma_0^2) \exp(-t^2/r_0^2) \sin(\omega t), \quad (3)$$

where $k = \omega/c$ is the laser pulse wave number in a vacuum. Eq. (3) gives the first order approximation to the longitudinal laser electric field. The VLPL numerical scheme (Pukhov, 1999) has the second order accuracy and propagates the fields according to the Maxwell equations. Figure 2 shows a *XY* cut of the E field and pulse intensity along the propagation direction inside the simulation box.

One immediately sees from Eq. (3) that the longitudinal electric field of the radially polarized laser pulse reaches its maximum on-axis. The phase of the longitudinal field is shifted by $\pi/2$ with respect to the transverse component (2). This means that a phase range exists, one per laser wavelength, where the longitudinal field is accelerating, and the transverse field is focusing.

The group velocity of the focused laser pulse is less than *c*. Thus, electron buckets trapped and accelerated in this phase range may overtake the laser pulse. If the laser pulse contains many cycles, already its relatively low intense foot wipes electrons away. The electrons will never experience the pulse maximum and the energy gain will be moderate. However, injection due to the ionization of deep levels of high-Z materials can provide an electron source at the pulse maximum. Singh (2006) described this as *self injection* of electrons.

In the first 3D PIC simulation, we take the radially polarized laser pulse (2)–(3) beam with the power of 100 PW (1 PW = 10^{15} W), 10 fs duration and the focal waist $\sigma_0 = 3\lambda$. The corresponding amplitude $eE_0/mc\omega = 1000$. Such (or stronger) laser pulses are expected within the extreme light infrastructure (ELI) project (ELI Project). Electron energy spectrum and angular distribution of the accelerated electrons are shown in Figure 3. Acceleration at petawatt powers is illustrated.

In the case of high *Z* atoms (xenon or copper), the maximum electron energies reached are significantly higher compared to hydrogen. The peak at the lowest energy

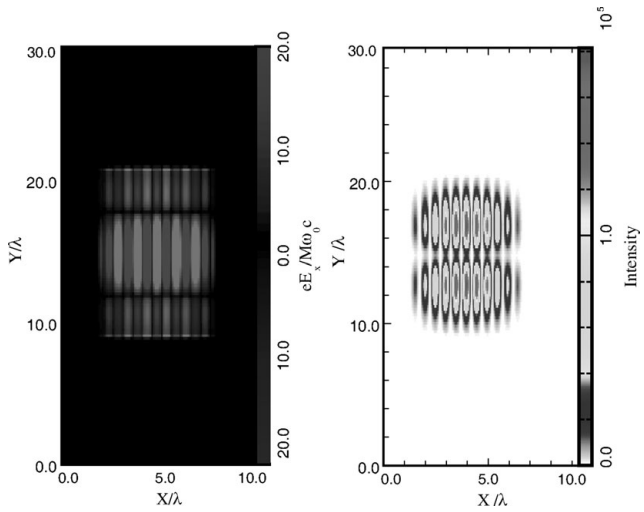

Fig. 2. *X-Y* cut of longitudinal field (E_x) (**a**) and intensity distribution (**b**) for the radially polarized laser pulse. Axes are in units of λ.

https://doi.org/10.1017/S0263034607000249 Published online by Cambridge University Press

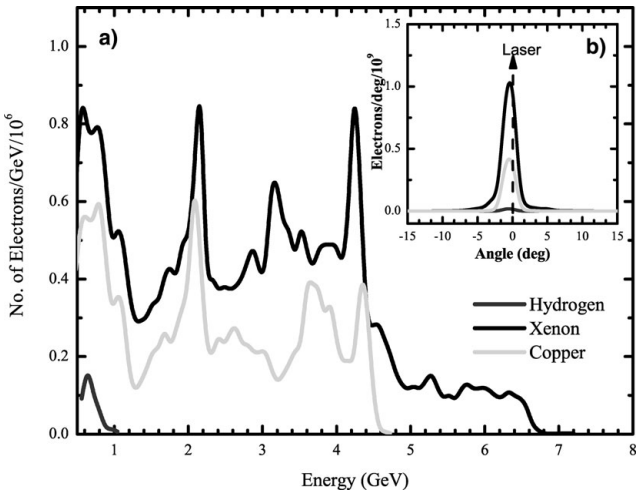

Fig. 3. (**a**) Electron energy spectrum (**b**) angular distribution of accelerated electrons for xenon, copper and hydrogen produced by the 100 PW, 10 fs radially polarized laser pulse with the focused field amplitude $eE_0/mc\omega = 1000$ and $\sigma_0 = 3\lambda$.

range corresponds to electrons extracted from the outer shells by the very foot of the pulse. The high energy peaks correspond to ionization of the deep electronic shells. For the angular distribution, we take electrons from the high energy peaks of the electron spectrum.

The maximum energies of the accelerated electrons reach $\sim$7 GeV for xenon and $\sim$5 Gev for copper. This difference is because xenon has deeper inner shells than copper with ionization potentials of those levels four times higher. We observe also a quasi-monoenergetic peak around 4.5 GeV containing some $\sim 10^6$ electrons per GeV. Looking at the degrees of ionizations of the atoms we observed Xe^{52+} and Cu^{27+} in this simulation.

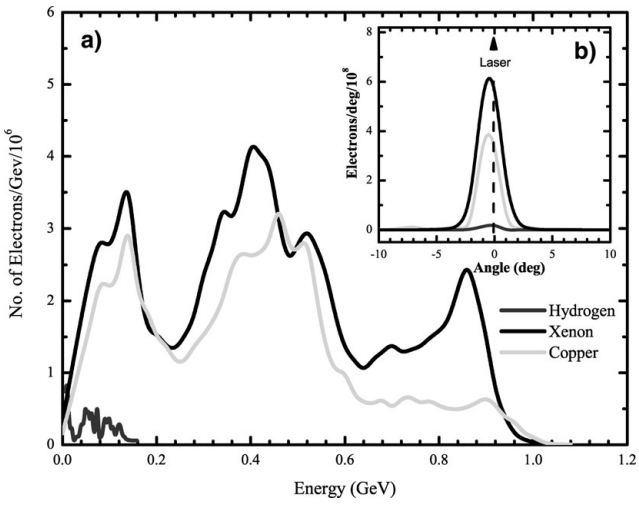

Fig. 4. (**a**) Electron energy spectrum and (**b**) angular distribution of accelerated electrons for xenon, copper and hydrogen produced by the 2 PW, 10 fs radially polarized laser pulse with the focused field amplitude $eE_0/mc\omega = 150$ and $\sigma_0 = 3\lambda$.

Figures 5 and 6a shows the properties of the high energy electron bunches as a one-dimensional on-axis cut (a) and as a 3D volume view (b). Both the results confirm that these are very short and highly compressed dense electrons bunches with attosecond shortness. The spikes in Figure 6a is the bunches in 3D volume view (Fig. 5), are around 100 attoseconds short.

To check how the acceleration process scales with the laser power, we performed an additional simulation with the laser pulse of $eE_0/mc\omega = 150$, that corresponds to a laser pulse with 2 PW. Results are shown in Figure 4. In this case, the electron energies reach GeV level, indicating the electron energy scaling as $E_{\max} \propto P^{1/2}$, where P is the laser power. In this simulation, we observed ionization up to Xe^{44+} and Cu^{27+}. Again, there is a drastic difference between the hydrogen target and the high-Z materials.

3.1.1. Single-cycle laser pulse

To get more insight on the performance of radially polarized laser pulses for electron acceleration, we did a further similar simulation with the 100 TW laser pulse, amplitude $eE_0/mc\omega = 100$, waist $\sigma_0 = \lambda$, and duration $T = \lambda/c$. The target material was hydrogen, so that the atoms were instantaneously ionized by the pulse foot. Figure 7 shows the electrons energy spectrum and angular distribution of the accelerated electrons for this case. One observes an excellent monoenergetic peak at 0.9 GeV. Electrons in this peak are collimated within a few degree opening angle. The 3D volume view, Figure 8, shows the single attosecond electron bunch.

The electron bunch length in the 1D on axis cut, Figure. 6b, is below 100 and is limited by the numerical spatial resolution of this simulation.

3.2. Acceleration by the Gaussian beam

In this section, we present simulation results for electron acceleration with the linearly polarized Gaussian laser pulse. The transverse electric field of the laser pulse at the

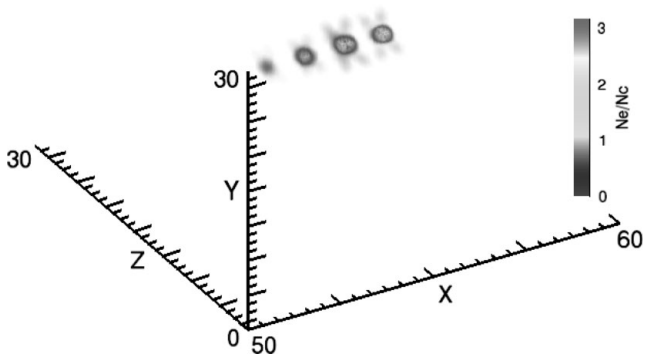

Fig. 5. Train of attosecond electron bunches produced by the 100 PW, 10 fs radially polarized laser beam for the xenon target after $t = 50$ laser cycles. The axes are in units of wavelength λ.

https://doi.org/10.1017/S0263034607000249 Published online by Cambridge University Press

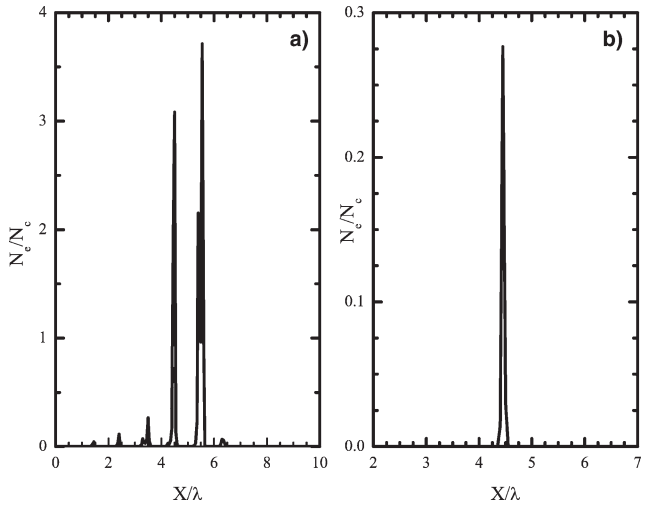

Fig. 6. 1D-cut of attosecond electron bunches. (**a**) 100 PW, 10 fs laser pulse, $eE_0/mc\omega = 1000$, $\sigma = 3\lambda$ with Xenon target, (**b**) single-cycle 100 TW laser pulse with $eE_0/mc\omega = 100$, $\sigma = \lambda$ and hydrogen target.

focal plane is

$$E_y = E_0 \exp(-r^2/\sigma_0^2) \exp(-t^2/T^2) \cos(\omega t), \quad (4)$$

where E_0, σ_0, $r = \sqrt{y^2 + z^2}$, and T have the same meaning as that of the radially polarized beam (2)–(3). The longitudinal component of the Gaussian beam at the focal plane is

$$E_x = -E_0 \frac{2y}{k\sigma_0} \exp(-r^2/\sigma_0^2) \exp(-t^2/T^2) \sin(\omega t). \quad (5)$$

Evidently, the longitudinal electric field component of the Gaussian pulse is zero on-axis and it reaches maximum at the pulse periphery.

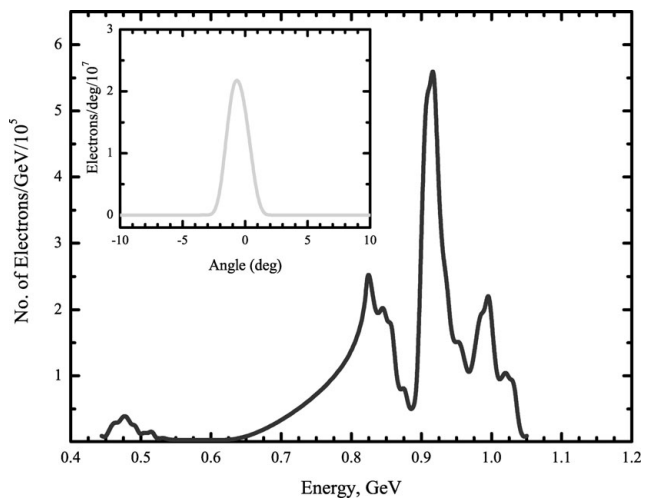

Fig. 7. Electron energy spectrum and angular distribution (inset) for the single cycle 100 TW laser pulse focused down to the amplitude $eE_0/mc\omega = 100$.

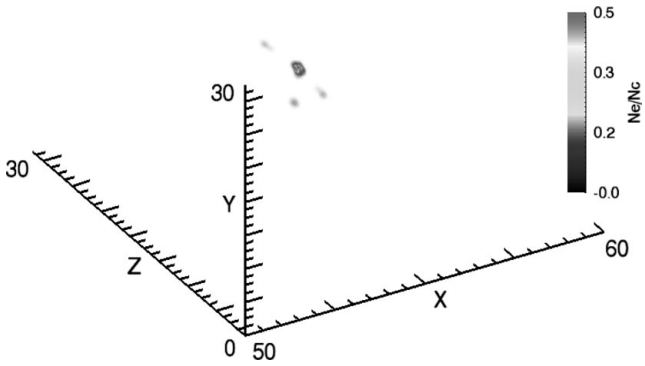

Fig. 8. 3D volume view of the single attosecond quasi-monoenergetic electron bunch produced by the single cycle radially polarized laser pulse after $t = 50$ laser cycles. The axes lengths are measured in the laser wavelength λ.

We perform two simulations with the Gaussian laser pulses. The powers of the Gaussian pulses correspond to those of the radially polarized ones, 100 PW and 2 PW.

The simulation results for these two case are presented in Figures 9 and 10. Evidently, electron acceleration with the Gaussian laser pulses is much less efficient and the accelerated electrons have large angular spread. Apparently, the effect of inner shell electron ionization does not improve the acceleration much, as the maximum energy reached by electrons of xenon or copper ions are not notably larger compared to that of hydrogen.

4. DISCUSSION

In the previous sections, we have shown that radially polarized laser pulses are suitable for acceleration of attosecond electron bunches to very high energies. The energy gain of

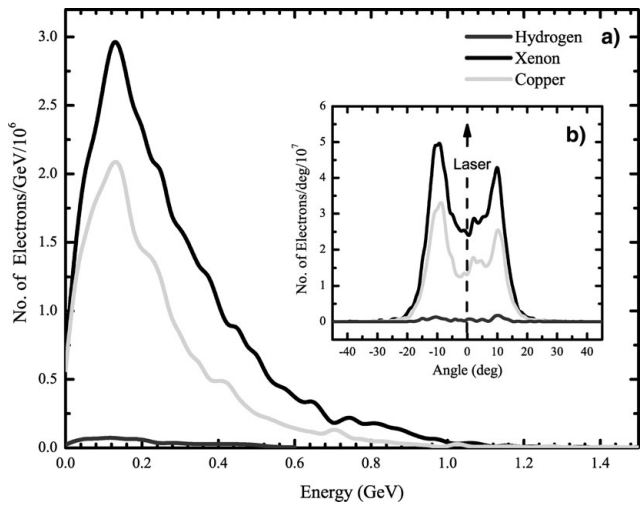

Fig. 9. (**a**) Electron energy spectrum and (**b**) angular distribution for xenon, copper and hydrogen targets for 100 PW, 10 fs Gaussian laser pulse with $\sigma_0 = 3\lambda$. Compare with the radially polarized pulse case, Figure 3.

https://doi.org/10.1017/S0263034607000249 Published online by Cambridge University Press

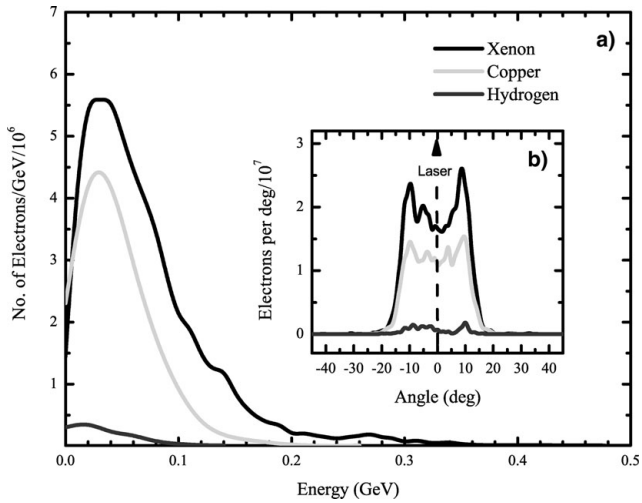

Fig. 10. (**a**) Electron energy spectrum and (**b**) angular distribution for xenon, copper and hydrogen targets for 2 PW, 10 fs Gaussian laser pulse with $\sigma_0 = 3\lambda$. Compare with the radially polarized pulse case, (Fig. 4).

electrons is given by the path integral

$$\int \mathbf{E}.d\mathbf{r}, \tag{6}$$

along the trajectory. We have seen that it is the longitudinal component of the radially polarized laser pulse (3) that accelerates the electrons. This component is on the order of $E_x \propto E_r/(k\sigma_0)$ and decays together with the laser pulse on the distance of the order of the Rayleigh length $Z_R = \pi\sigma_0^2/\lambda$. Thus, the estimate for the energy gain is

$$\Delta W \propto E_x \cdot Z_R \propto E_R\sigma_0 \propto \sqrt{P}, \tag{7}$$

where P is the laser pulse power. This estimate agrees well with the simulation results.

ACKNOWLEDGEMENT

This work was supported by DFG in the frames of Transregio TR18.

REFERENCES

Ammosov, M.V., Delone, N.B. & Krainov, V.P. (1986). Tunnel ionization of the complex atoms and of atomic ions in an alternating electromagnetic field. *Sov. Phys. JETP* **64**, 1191–1194.

Augst, S., Meyerhofer, D.D., Strickland, D. & Chin, S.L. (1991). Laser ionization of noble gases by Coulomb-barrier suppresion. *J. Opt. Soc. Am.* B8 858–867.

Bahk, S.W., Rousseau, P., Planchon, T.A., Chvykov, V., Kalintchenko, G., Maksimchuk, A., Mourou, G.A. & Yanovsky, V. (2005). Characterization of focal field formed by a large numerical aperture paraboloidal mirror and generation of ultra-high intensity (10^{22} W/cm^2). *Appl. Phys. B.* **80**, 823–832.

Carlson, T.A., Nestor, C.W., Wasserman, N. & McDowell, J.D. (1970). Calculated ionization potentials for multiply charged ions. *Atomic Data* **2**, 63–69.

ELI – Extreme Light Infrastructure, *European Project–http://www.eli-laser.eu*

Faure, J., Glinec, Y., Pukhov, A., Kiselev, S., Gordienko, S. Lefebvre, E., Rousseau, J.P., Burgy, F. & Malka, V. (2004). A laserplasma accelerator producing monoenergetic electron beams. *Nature* **431**, 541–544.

Fuerbach, A., Fernandez, A., Apolonski, A., Fuji, T. & Krausz, F. (2005). Chirped-pulse oscillators for the generation of high-energy femtosecond laser pulses. *Laser Part. Beams* **23**, 113–116.

Gedder, C.G.R., Toth, Cs., Tilborg, J. Van., Esarey, E., Schroeder, C.B., Bruhwiler, D., Nieter, C., Cary, J. & Leemans, W.P. (2004). High-quality electron beams from a laser wakefield accelerator using plasma-channel guiding. *Nature* **431**, 538–541.

Glinec, Y., Faure, J., Pukhov, A., Kiselev, S., Gordienko, S., Mercier, B. & Malka, V. (2005). Generation of quasi-monoenergetic electron beams using ultrashort and ultraintense laser pulses. *Laser Part. Beams* **23**, 161–166.

Hu, S.X. & Starace, A.F. (2002). GeV electrons from ultraintense laser interaction with highly charged ions. *Phys. Rev. Lett.* **88**, 245003.

Hu, S.X. & Starace, A.F. (2006). Laser acceleration of electrons to giga-electron-volt energies using highly charged ions. *Phys. Rev.* **E73**, 066502.

Kawata, S., Kong, Q., Miyazaki, S., Miyauchi, K., Sonobe, R., Sakai, K., Nakajima, K., Masuda, S., Ho, Y.K., Miyanaga, N., Limpouch, J. & Andreev, A.A. (2005). Electron bunch acceleration and trapping by ponderomotive force of an intense short-pulse laser. *Laser Part. Beams* **23**, 61–67.

Keldysh, L.V. (1965). Ionization in the field of a strong electromagnetic wave. *Sov. Phys. JETP* **20**, 1307–1314.

Koyama, K., Adachi, M., Miura, E., Kato, S., Masuda, S., Watanabe, T., Ogata, A. & Tanimoto, M. (2006). Monoenergetic electron beam generation from a laser-plasma accelerator. *Laser Part. Beams* **24**, 95–100.

Leemans, W.P., Nagler, B., Gonsalves, A.J., Toth, Cs., Nakamura, K., Geddes, C. G. R., Esarey, E., Schroeder, C.B. & Hooker, S.M. (2006). GeV electron beams from a centimetre-scale accelerator. *Nature Phys.* **2**, 696–699.

Lifschitz, A.F., Faure, J., Glinec, Y., Malka, V. & Mora, P. (2006). Proposed scheme for compact GeV laser plasma accelerator. *Laser Part. Beams* **24**, 255–259.

Mangles, S.P.D., Murphy, C.D., Najmuddin, Z., Thomas, A.G.R., Collier, J.L., Dangor, A.E., Divall, E.J., Foster, P.S., Gallacher, J.G., Hooker, C.J., Jaroszynski, D.A., Lanhley, A.J., Mori, W.B., Norreys, P.A., Tsung, F.S., Viskup, R., Walton, B.R. & Krushelnick, K. (2004). Monoenergetic beams of relativistic electrons from intense laserplasma interactions. *Nature* **431**, 535–538.

Pukhov, A. (1999). Three-dimensional electromagnetic relativistic particle-in-cell code VLPL (Virtual Laser Plasma Lab). *J. Plasma Phys.* **61**, 425–433.

Pukhov, A. & Meyer-Ter-Vehn, J. (2002). Laser wake field acceleration: the highly non-linear broken-wave regime. *J. Appl. Phys.* **B74**, 355–361.

Pukhov, A. (2003). Strong field interaction of laser radiation. *Rep. Prog. Phys.* **66**, 47–101.

Salamin, Y. (2007). Mono-energetic GeV electrons from ionization in a radially polarized laser beam. *Optics. Lett.* **32**, 90–92.

Singh, K.P. (2006). Self-injection and acceleration of electrons during ionization of gas atoms by a short laser pulse. *Phys. Plasmas* **13**, 043101.

Strickland, D. & Mourou, G (1985). Compression of amplified chirped optical pulses. *Opt. Commun.* **56**, 219.

Varin, C. & Piche, M. (2002). Acceleration of ultra-realtivistic electrons using high intensity TM_{01} laser beams. *App. Phys., B* **74**, S83–S88.

Yin, L., Albright, B.J., Hegelich, B.M. & Fernndez, J.C. (2006). GeV laser ion acceleration from ultrathin targets: The laser break-out afterburner. *Laser Part. Beams* **24**, 291–298.

https://doi.org/10.1017/S0263034607000249 Published online by Cambridge University Press